Since January 2020 Elsevier has created a COVID-19 resource centre with free information in English and Mandarin on the novel coronavirus COVID-19. The COVID-19 resource centre is hosted on Elsevier Connect, the company's public news and information website.

Computers in Biology and Medicine 135 (2021) 104613

Contents lists available at ScienceDirect

Computers in Biology and Medicine

journal homepage: www.elsevier.com/locate/compbiomed

In *silico* investigation on the inhibitory effect of fungal secondary metabolites on RNA dependent RNA polymerase of SARS-CoV-II: A docking and molecular dynamic simulation study

Kosar Sadat Ebrahimi [a], Mohabbat Ansari [b], Mahdieh S Hosseyni Moghaddam [c], Zohre Ebrahimi [d], Zohre salehi [e], Mohsen Shahlaei [e,**], Sajad Moradi [a,*]

[a] Nano Drug Delivery Research Center, Health Technology Institute, Kermanshah University of Medical Sciences, Kermanshah, Iran
[b] Department of Tissue Engineering and Applied Cell Science, School of Advanced Technologies in Medicine, Shahid Beheshti University of Medical Sciences, Tehran, Iran
[c] Department of Plant Pathology, Faculty of Agriculture, Tarbiat Modares University, Tehran, Iran
[d] Department of Ophthalmology, School of Medicine, Farabi Eye Hospital, Tehran University of Medical Sciences, Tehran, Iran
[e] Medical Biology Research Center, Health Technology Institute, Kermanshah University of Medical Sciences, Kermanshah, Iran

ARTICLE INFO

Keywords:
Covid-19
Secondary metabolite
Endophytic fungi
Molecular modeling
Protein structure

ABSTRACT

The newly emerged Coronavirus Disease 2019 (COVID-19) rapidly outspread worldwide and now is one of the biggest infectious pandemics in human society. In this study, the inhibitory potential of 99 secondary metabolites obtained from endophytic fungi was investigated against the new coronavirus RNA-dependent RNA polymerase (RdRp) using computational methods. A sequence of blind and targeted molecular dockings was performed to predict the more potent compounds on the viral enzyme. In the next step, the five selected compounds were further evaluated by molecular dynamics (MD) simulation. Moreover, the pharmacokinetics of the metabolites was assessed using SwissADME server. The results of molecular docking showed that compounds 18-methoxy cytochalasin J, (22E,24R)-stigmasta-5,7,22-trien-3-β-ol, beauvericin, dankasterone B, and pyrrocidine A had higher binding energy than others. The findings of MD and SwissADME demonstrated that two fungal metabolites, 18-methoxy cytochalasin J and pyrrocidine A had better results than others in terms of protein instability, strong complex formation, and pharmacokinetic properties. In conclusion, it is recommended to further evaluate the compounds 18-methoxy cytochalasin J and pyrrocidine A in the laboratory as good candidates for inhibiting COVID-19.

1. Introduction

In December 2019, a case of unknown pneumonia was reported in Wuhan, China, which rapidly spread around the world and resulted in a big pandemic. The causative agent was soon revealed as a coronavirus identified by the World Health Organization as a 2019 novel coronavirus (2019-nCoV). It was named severe acute respiratory syndrome Coronavirus 2 (SARS-CoV-2) by the International Committee on Taxonomy of Viruses [1]. The disease not only causes direct tissue damage but can also lead to extrapulmonary manifestations by affecting the endothelium, evoking thrombosis, dysregulating the immune responses, and causing the incompatibility of the pathways related to angiotensin-converting enzyme 2. Consequently, thrombotic complications, arrhythmia, myocardial dysfunction, acute coronary syndromes, acute kidney injury, gastrointestinal symptoms, hepatocellular injury, hyperglycemia, ketosis, as well as dermatologic and neurologic complications [2] might occur. In addition, ocular symptoms, such as congestion, dry eye, and blurred vision due to retinal and corneal involvement have been reported [3].

Coronaviruses are positive single-stranded RNA viruses and have the largest genome among all RNA viruses with a length of approximately 30 Kbp [4]. The ORF1a and ORF1ab are responsible for encoding polyproteins 1a (pp1a) and 1 ab (pp1ab), respectively, and together encode 16 nonstructural proteins (nsp1-nsp16). The other four ORFs are located at the 3' end of the viral genome and encode four structural proteins, namely Spike (s), Membrane (m), Envelope (E), and Nucleocapsid (N)

* Corresponding author.
** Corresponding author. Department of Medicinal Chemistry, Faculty of Pharmacy, Kermanshah University of Medical Sciences, 67346-67149, Kermanshah, Iran.
E-mail addresses: mohsenshahlaei@yahoo.com, mshahlaei@kums.ac.ir (M. Shahlaei), sajadmoradi28@gmail.com, sajad.moradi@kums.ac.ir (S. Moradi).

https://doi.org/10.1016/j.compbiomed.2021.104613
Received 25 February 2021; Received in revised form 27 June 2021; Accepted 27 June 2021
Available online 5 July 2021

[5]. The RNA-dependent RNA polymerase (RdRp) complex of SARS-CoV-2 consists of the core non-structural protein 12 (pp1ab) and their co-factors nsp 7 and nsp8 (pp1a). It is the key enzyme for the replication and transcription of a virus and could be considered as the bottleneck for controlling viral proliferation [6].

The structure of nsp12 seems a right-hand cup comprised of two main domains, including nucleotidyltransferase (Ni RAN) (residues Q117-A250) and the N-terminal domain of nidovials, which consists of N-terminal B hairpin (residues 31–50). These are connected to the c terminal domain by another interface domain (residues L251-R365) [7]. The C-terminal domain (residues 366–932), including three subdomains of the finger (residues L366-A581 and K621-G679), palm (residues T582-P620 and T680-Q815), and thumb (residues H816-E920) and altogether carry out RNA polymerization [8]. The active site of the enzyme is formed by a complex of the structurally conserved motifs A, B, C, D, E, F, and G, of which motifs A to E are located in the palm subdomain and motifs F and G are in the finger subdomain. The catalytic activity of the enzyme is attributed to the four aspartate residues of Asp 618 and Asp 623 from motif A along with residues Asp 760 and Asp 761 from motif C [9].

Repurposing the approved medications is one of the most common options to overcome the disease in such infectious epidemics with no indicated medications because of the needed labor, as well as the time-consuming and costly procedures of introducing new medicines. Another approach is investigating the natural medicinal compounds that can be readily and rapidly prepared on a large scale. Fungal endophytes are endosymbiosis organisms that live on the plants without inducing physiological disorder in their hosts [10]. In such plants, commonly at the endophytes-hosts interaction site, specific secondary metabolites are produced either by the host or the endophytes. Hundreds of these compounds have been reported as bioactive agents and have shown significant therapeutic properties, such as anticancer, antibiotic, anti-parasitic, antiviral, antidiabetic, neuroprotective, and immunosuppressive impacts [11]. The large-scale production of these compounds is much easier than chemical ones. Furthermore, many of these valuable medications cannot be produced in chemical laboratories due to the complexity of their molecular structures [12]. Natural secondary metabolites from fungal endophytes have a wide range of biological activities and can be structurally classified into several categories including, namely isocoumarins, alkaloids, steroids, flavonoids, lignans, glycosides, xanthones, quinones, phenylpropanoids, aliphatic metabolites, terpenoids, and lactones [13].

Mathematically, there are several types of molecular computational approaches of which the classical methods can be used in biology and studies on proteins because of the potential to address many particle systems. In this case, two techniques of molecular docking and molecular dynamic simulation are utilized for predicting the interaction site and dynamics of the interaction, respectively. These techniques help to screen the biological activity of diverse potentially active compounds in a cost- and time-effective in silico manner [14,15]. Molecular modeling methods are nowadays applied in various fields of science, especially in drug design and discovery [16–18]. With the rising of the new coronavirus pandemic, numerous studies have computationally investigated the interaction and inhibitory effects of approved medications or natural medicinal compounds against specific targets in Coronavirus disease 2019 (COVID-19) [19–23].

In this study, using docking and molecular dynamic simulation, the interactions and potent inhibitory effects of some important fungal secondary metabolites were investigated on SARS-CoV-2 nsp12. After two steps of molecular docking, the more potent compounds were evaluated in terms of their effects on the structure and dynamic of the protein. Finally, after the exploration of their pharmacological aspects, the best metabolites are introduced for further experimental studies.

Table 1
The final result of targeted molecular docking.

Compound	Lowest binding energy (kcal/mol)	Number of runs in cluster
10-deacetylbaccatin III	−7	117
18-ethoxycytochalasin	**−10.2**	**186**
2-phenylethyl 1H-indol-3-yl-acetate	−8/39	101
(22E,24R)-stigmasta-5,7,22-trien-3-β-ol	**−9.91**	**128**
Alternariol	−7.6	145
Alternariol 9-methyl ether	−8.5	115
Altertoxin I	−8.36	134
Altertoxin II	−7.52	100
Altertoxin III	−6.58	158
Altertoxin V	−8.91	164
Beauvericin	**−10.14**	**123**
Dankasterone B	**−9.87**	**152**
Jammosporin A	−7.8	124
Naphthoquinone (Herbarin)	−6.51	113
Outovirin C	−8.6	148
Periconiasin D	−9.1	109
Phomocytochalasin	−7.35	178
Purpureone	−8.9	198
Pyrrocidine A	**−11.3**	**124**
Taxol	−8.53	143
Thielavins A	−7.36	109
Thielavins J	−8.65	172
Viriditoxin	−6.35	130
α -Viridin	−7.56	186
β-Viridin	−8.11	210

2. Methods

2.1. Preparation of the molecular structures

The three-dimensional structure of the protein (RdRp) was taken from protein data bank (www.rcsb.org) (PDB.ID 6nur). To preparing the Molecular structures of fungal secondary metabolites (Table S1) at first their 2D chemical conformations were sketch by ChemSketch tool of ACD/LAB package (www.acdlabs.com). The 2D structures were then transferred to the Avogadro package and steep algorithm was used to minimize energy and optimize their conformation.

2.2. Docking studies

Molecular docking as one of the sub-techniques of molecular modeling is a key tool in structural molecular biology and computer aided drug design. The docking studies were done in autodock –autogrid package in two sequential steps. At the first a blind docking were done on whole protein structure. The structures which attached to the active site with the binding energy >6 kcal/mol were then selected for second step of targeted docking. First, the polar hydrogens and gasteiger charges were computed and added to the structure for all molecules using MGLtools package [24]. All bonds set as active for ligands and energetic maps were calculated for each of the respective atom types in autogrid 4. In the blind docking step, the search spaces were big enough in order to all of the protein was accessible for ligand binding. In the targeted docking, the search spaces were set on the active site of enzyme. Finally for all compounds, 250 runs of molecular dockings were done under the Lamarckian genetic algorithm [25].

The five obtained bonded ligand with the lowest energy and maximum number of runs in the cluster were selected for further analyzing by molecular dynamic simulations.

2.3. Molecular dynamic simulation

To investigate the dynamic of interactions between ligands and protein, the molecular dynamic simulation (MDs) approach were

Table 2
The most potent metabolites extracted from molecular docking studies.

compound	Endophytic fungi	Host plant	References
18-methoxy cytochalasin J	Phomopsis sp.	Garcinia kola	Jouda et al. (2016)
(22E,24R)-stigmasta-5,7,22-trien-3-β-ol	Aspergillus terreus	Carthamus lanatus	Elkhayat et al. (2016)
Beauvericin	Epicoccum nigrum	Entada abyssinica	Dzoyem et al. (2017)
Dankasterone B	Phomopsis theicola	Litsea hypophaea	Hsiao et al. (2016)
Pyrrocidine A	Neonectria ramulariae	Cylindrocarpon sp. and Acremonium zeae	Uesugi et al. (2016)

utilized by using computational package of *Gromacs* (version2018). Five selected Protein-ligand complexes from the 2nd docking step (Table 2) were chosen for further interaction analysis in molecular dynamics. The Topology information for protein and ligands were respectively obtained in gromos53a6 force field [26] and *PRODRG* server [27]. Simulation boxes were solvated by SPC/E water [27] and by adding the appropriate amount of counter ion, all systems were neutralized. In order to eliminating atomic clashes in the system, energy minimization were done using the steepest descend algorithm until the energy reaches below the 10 kj/mol [28]. Periodic boundary condition was applied on all boxes and in all directions of X, Y and Z. Temperature and pressure were coupled to 310 K and 1 bar in NVT and NPT ensembles, respectively. In these cases the V-rescale thermostat was used for temperature and a parinello-rahman barostat was applied for pressure equilibrations. Electrostatic and van der Waals (vdW) non-bonded interactions were also calculated both in the cut-off range of 1 nm. The bond constraint for all heavy atoms was done by using the LINCS algorithm [29]. Finally, 100 ns of MD simulations were performed under the leap frog method [30]. Interaction energies between the ligands and protein in the dynamic state were calculated using Molecular Mechanics Poisson-Boltzmann Surface Area (MMPBSA) method [31]. Graphical representations and 2D molecular interactions were prepared in *VMD* (https://www.ks.uiuc.edu/Research/vmd) and *LigPlot* [32], respectively. The pharmacokinetic parameters were obtained from *SwissADME* server (http://www.swissadme.ch). Eventually the toxicity of the fungal metabolites was predicted in the *ProTox-II* webserver [33].

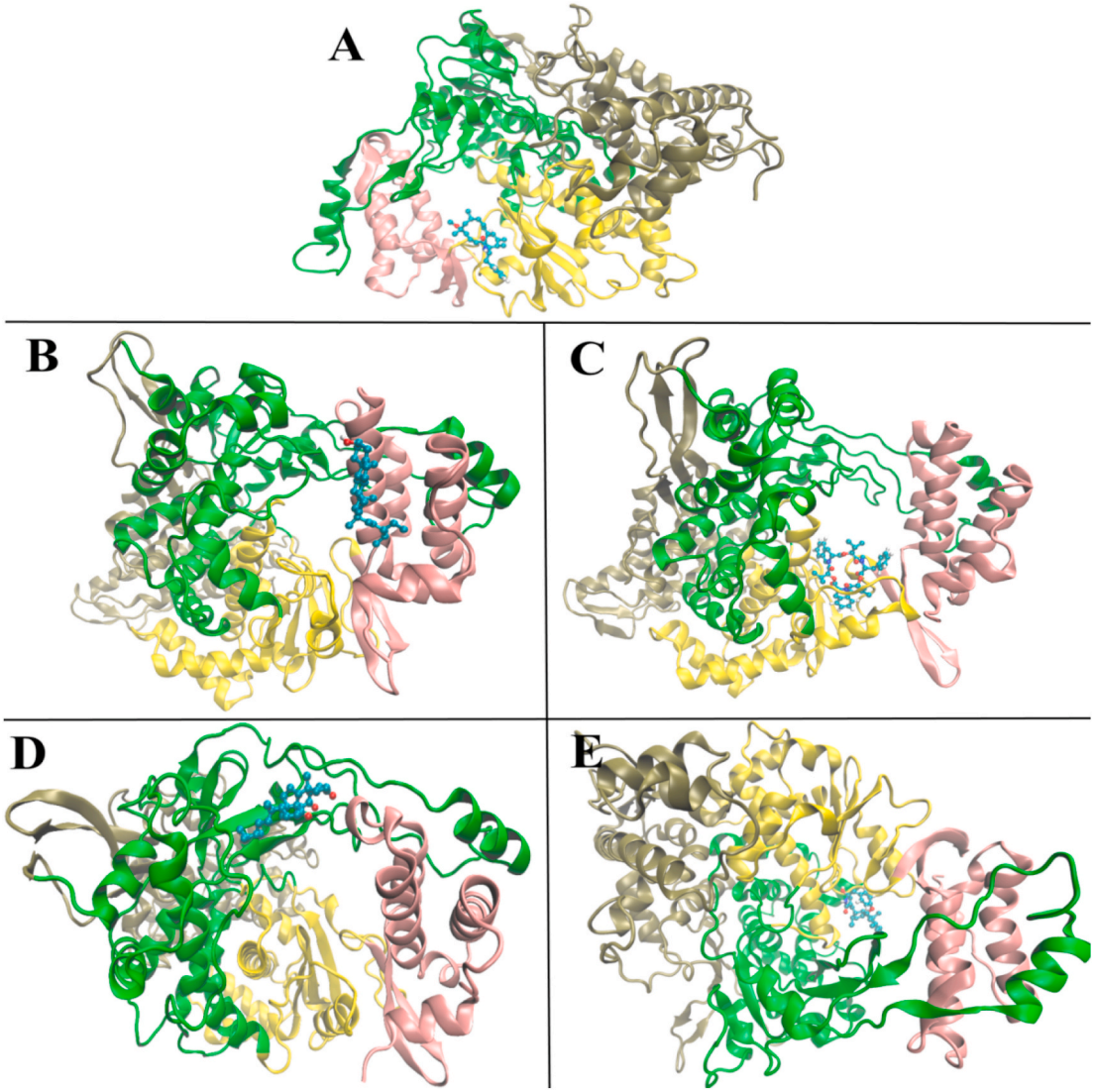

Fig. 1. Three-dimensional representation of interaction between candidate compounds and viral polymerase; A) 18-methoxy cytochalasin J, B) (22E, 24R)-stigmasta-5,7,22-trien-3-β-ol, C) beauvericin, D) dankasterone B and E) pyrrocidine A. Finger (green), Palm (yellow), Thumb (pink).

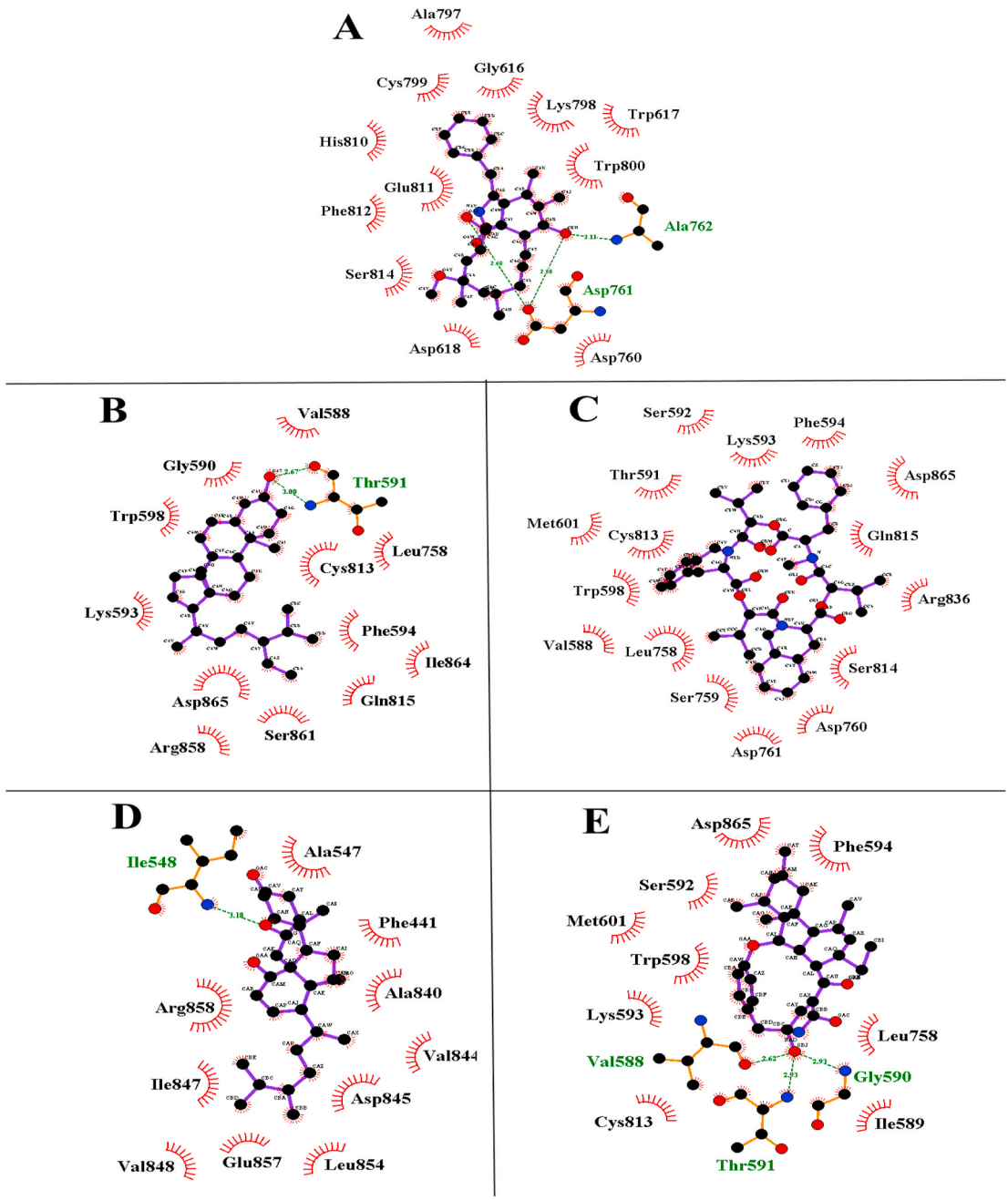

Fig. 2. Two-dimensional representation of interactions between candidate compounds and viral polymerase; A) 18-methoxy cytochalasin J, B) (22E, 24R)-stigmasta-5,7,22-trien-3-β-ol, C) beauvericin, D) dankasterone B and E) pyrrocidine A. (The hydrophobic interactions are represented as "crenate" and the h-bonds are shown by green dotted line).

3. Results

3.1. Docking studies

Molecular docking provides information about where and how a ligand binds to a macromolecule, such as a protein. Among the 99 blind docked compounds in step one, those with a binding energy of >6 kcal/mol to the active site were selected for another targeted docking. Therefore, in step two, 25 compounds, which met the criterion were docked to the active site of nsp12. The results for the second step of molecular docking are represented in Table 1.

Using the results of the second docking experiment, 5 of the 25 compounds with higher binding energy and cluster rank were selected for the further molecular dynamic study. Biological details of the final five fungal metabolites are summarized in Table 2. Moreover, three- and two-dimensional schematics of the interaction for selected complexes are represented in Figs. 1 and 2.

As can be seen in Figs. 2 and 18-methoxy cytochalasin j (MCJ) has formed three strong hydrogen bondings with Asp761 and Ala762 in catalytic motif C (Fig. 2A) [23]. This can make severe negative effects on the catalytic activity of the enzyme. In addition, the ligand has an interaction with residues His810, Glu811, Phe812, and Ser814 in motif E. As motif E is involved in stabilizing primer strand in the active site [23], the drug interaction with this site can significantly prevent correct RNA-enzyme complex formation. In terms of (22E,24R)-stigmasta-5,7,22-trien-3-β-ol (STB), almost all interacted residues belong to the palm subdomain (Fig. 2B). The main role of this subdomain is forming the catalytic site, the interaction of which with medication can deform its

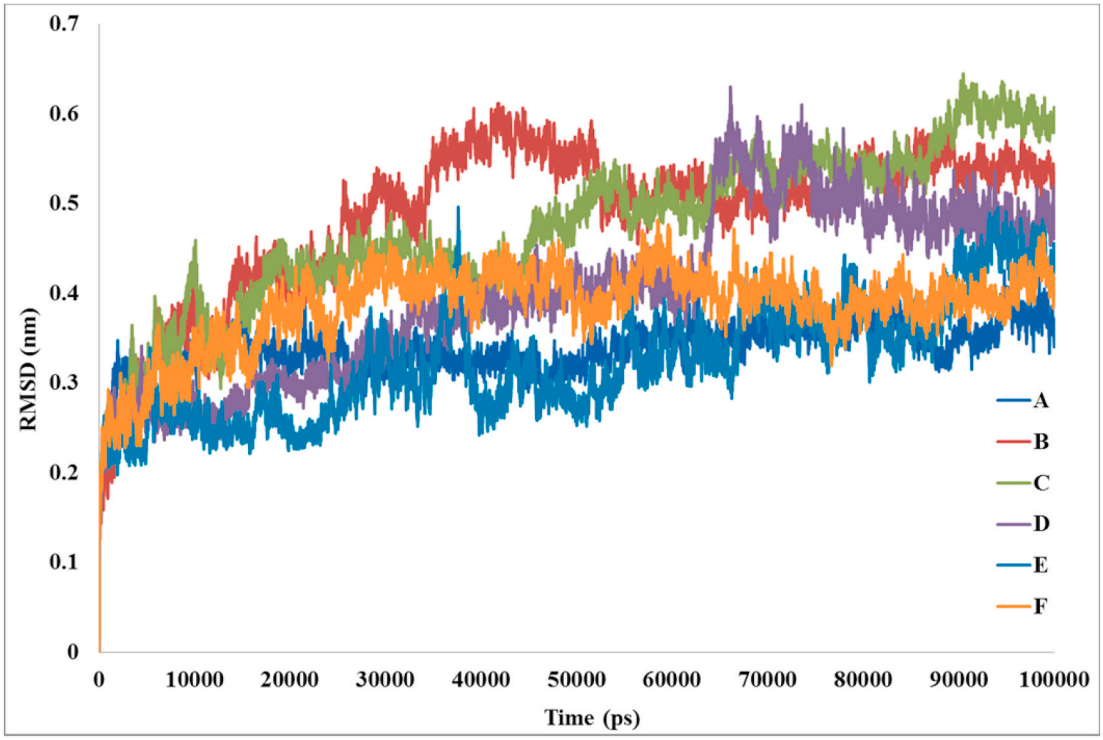

Fig. 3. The changes in *RMSD* values for (A) free protein, (B) Protein-18-methoxy cytochalasin J, complex C) Protein- (22E,24R)-stigmasta-5,7,22-trien-3-β-ol complex, (D) Protein-beauvericin complex, (E) Protein-dankasterone b complex and (F) Protein-pyrrocidine A complex.

arrangement leading to malfunction in the catalytic activity of the enzyme [34]. Beauvericin forms a stable hydrogen bond with Cys813 which is located at the motif E of the palm subdomain with its role being to monitor the correct positioning of the end of the primer (Fig. 2C) [34]. Other residues involved in the interaction with this compound entail Phe812, Leu758, Val587, Leu602, Val588, Trp598, Thr586, Gly597, Gly596, Met601, Ser592, Lys593, Ser814, Asp865, Tyr689, and Ala688. Two residues Cys813 and Phe812 exist in the motif E of the palm subdomain and their interaction with ligands can lead to the disruption of the RNA-enzyme complex. Dankasterone B forms a hydrogen bonding with residue Tyr545 in the motif F of the finger subdomain. It also forms a Van der Waals bond with Ser501, Gln541, ile847, Asp846, Lys545, and Lys411 (Fig. 2D). As the metabolite is in direct interaction with Lys545, it can be concluded that in addition to loosening the template bond to protein, dankasterone B can also impair the positioning of incoming nucleotides. Pyrrocidine A establishes two hydrogen bonds with Ser759 and interacts with amino acids Phe594, Ser592, Lys593, Cys813, Gly590, Leu758, Ala688, and Thr591 (Fig. 2E). The Cys813 is located at the motif E of the palm subdomain, the role of which is to monitor the correct positioning of the primer. The binding of pyrrocidine A to this residue can prevent or impair the initiation of polymerization. These results demonstrate that the binding of the selected fungal metabolites to the active site of the enzyme might have potentially disrupted RNA-enzyme complex formation preventing the RdRp to start polymerization and impairing the catalytic activity.

3.2. Molecular dynamic simulations

Molecular dynamics simulation is one of the best methods to investigate the dynamic behavior of macromolecules at the molecular and atomic levels. Nowadays, this approach is used extensively in drug discovery and the formulation of medications worldwide. In order to evaluate the dynamics of drug-protein complexes and investigate the influences of such interactions on the structure and dynamics of protein, all final complexes of metabolite-RdRp were examined by 50 ns of MD simulations. As the first analysis of the MD trajectories, the change in the values of root-mean-square deviation (RMSD) was evaluated for protein atoms in the simulation. It can be understood from the pattern of the RMSD diagram whether the system reached an equilibrated state or not. Most of the data were obtained in the equilibrated state of the systems. Consequently, the results of the RMSD analysis also determine whether the simulation time was enough or not. The plateau diagram of this analysis for free protein indicated that the simulation time was sufficient for this protein in this condition. The analysis was performed on all understudy systems and their results are represented in Fig. 3. In the case of free protein after an initial jump due to the relaxation of the protein, the system reached equilibration after 10 ns and fluctuated around the mean RMSD value of 0.3 nm until the end of the simulation. This finding confirmed the sufficiency of simulation time, in addition to indicating that there is no significant change in protein structure during simulation. The RMSD diagram of RdRp in the complex with 18-MCJ was the most different pattern from those of free protein in the terms of RMSD value.

Comparatively, the most remarkable fluctuations in the value of RMSD occurred in the system containing dankasterone B showing the highest degree of instability in the protein structure. The patterns of protein interaction are almost identical with the other three with moderate fluctuations and the mean value of 0.4 nm at the end of the simulation.

Root-mean-square fluctuation (RMSF) is an analysis for evaluating the fluctuation values of all amino acids in the protein. It is a standard deviation of displacements of each amino acid related to the sum of protein displacement. The more RMSF the more unsteady amino acids are and vice versa. The value for each amino acid can revolve due to protein interaction with a ligand. Attaching of all fungal metabolites to the viral RdRp has changed the RMSF of protein residues in diverse parts of the protein (Fig. 4). In the case of 18-MCJ, in most parts of protein, especially at the locations around residues 224–232, 252–290, 308–330, 367–380, 410–458, 485–495, 520–560, 570–610, 630–660, and 680–688 the residue fluctuation elevated significantly. In contrast, in some residue locations, including 137, 302, 503, 556–570, 614–620,

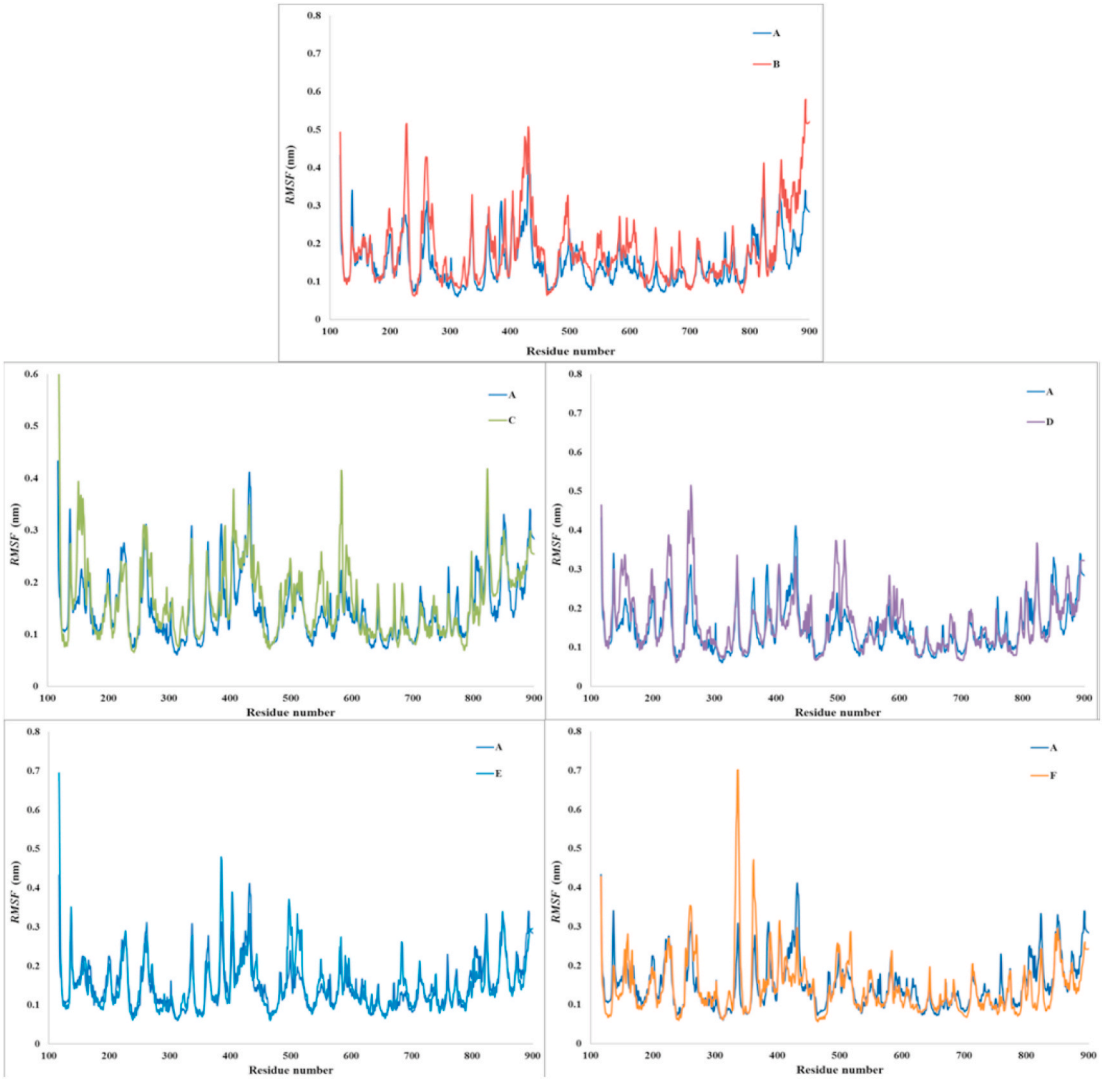

Fig. 4. Comparison of changes in *RMSF* value of protein in interaction with different ligands; (A) free protein, (B) Protein-18-methoxy cytochalasin J, (C) Protein-(22E,24R)-stigmasta-5,7,22-trien-3-β-ol, (D) Protein-beauvericin, (E) Protein-dankasterone B, and (F) Protein-pyrrocidine A.

725–735, 759, and 806–810 the RMSF decreased after the binding of protein to the ligand. These results may indicate that the binding of 18-MCJ to protein increases the RMSF value of interface domain, finger, motif F, and motif B in the palm subdomain. The diminished value of RMSF in protein was observed at residue positions 558–570, 614–620,725-735, and 806–810 in the palm subdomain. In the case of (22E,24R)-stigmasta-5,7,22-trien-3-β-ol, fluctuation increased in residues 151–155 (N-terminal domain) 546–549, 579–609, and 643–683 (in finger subdomain), decreased in residues 124–138, 198, 221–226 (N-terminal domain) 712–715, and 759–790 (palm subdomain). Elevated amino acid fluctuations in the beauvericin-RdRp complex were seen in amino acids 144–162, 150–158, 225–237, (N-terminal domain), 320–326 (interface domain), 494–506 (finger subdomain), and 564–600 (palm subdomain). Reductions were observed in the fluctuations of residues 361–390, 410–432 (finger subdomain), and 657–675, 776–791 (palm subdomain). In the case of dankasterone B, augmented RMSF value was found in 383–388, 403, and 546–548 (finger subdomain), as well as 581–596 and 678–686 (palm subdomain). Moreover, most decreased fluctuations were seen in residues 124–133, 142–213 (N-terminal domain), 275–318 (interface domain) 332–376, 409–435, 449–491, and 644–670 (finger subdomain). In the case of pyrrocidine A, an increased RMSF was revealed in some residues, including 160–167, 171–226 (N-terminal domain), 252–272, 318–368 (interface domain), 511–519, 549 (finger subdomain), 584, and 642–682 (palm subdomain). On the other hand, fluctuations decreased in most of the protein residues at locations 122–157, 238–248 (N-terminal domain), 383–386, 416–434, and 462–489 (finger subdomain), as well as 580–625 and 688–708 (palm subdomain). As it is clear, the binding of ligands to RdRp has changed the fluctuation values of the residues involved in RNA binding or the catalytic activity of nsp12. Practically, these events can disrupt the polymerase activity of RdRp and impair the proliferation of new infectious virions.

The radius of gyration (Rg) is an index of the overall mean dimension of protein. An increase and/or decrease in this parameter indicates the loosing or compression of the molecular structure of a macromolecule. It is expected that the compactness of the structure of enzymes exerts a great effect on the quality of the substrate binding to the active site. The results of changes in the Rg of proteins bonded to different ligands are shown in Fig. 5. As could be seen in this figure, the free protein has slightly compressed and fluctuates around an Rg of 2.86 nm. In comparison with free protein, the Rg value of nsp12 in all complexed systems except those containing beauvericin declined significantly, which is a sign of compression in protein structure after binding to ligands. In terms of the fluctuations of Rg value resulting from alternate loosing-compression in the protein structure, high fluctuation can be seen in the Rg diagrams of a protein complex with MCJ, DNB, PYR, and BVC.

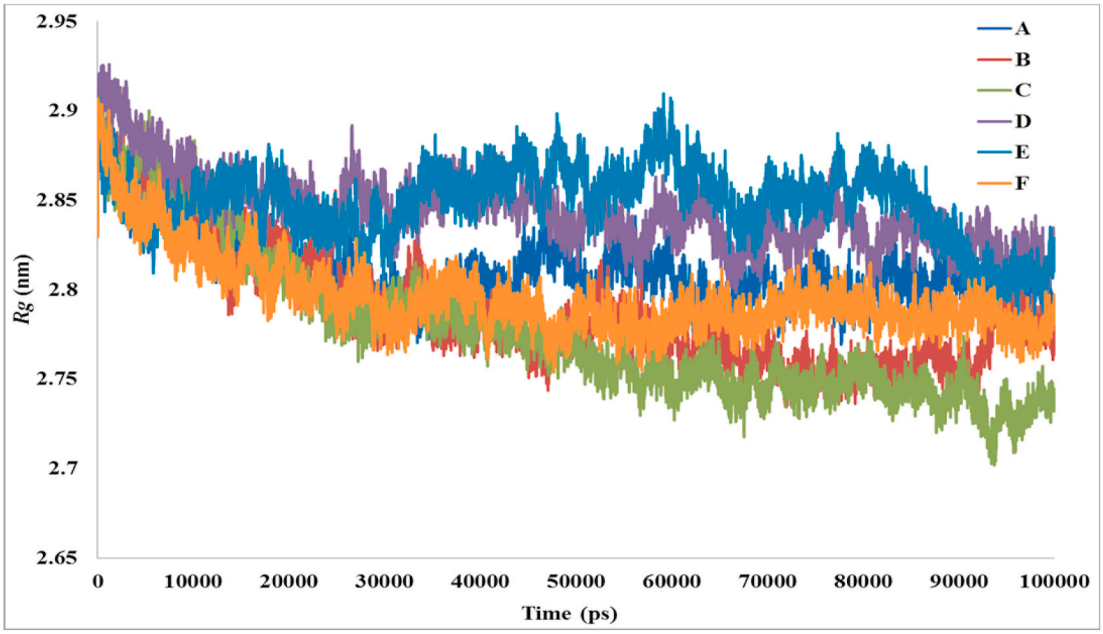

Fig. 5. Comparison of changes in Rg value of protein in interaction with different ligands (A) free protein, (B) Protein-18-methoxy cytochalasin J, (C) Protein-(22E,24R)-stigmasta-5,7,22-trien-3-β-ol, (D) Protein-beauvericin, (E) Protein-dankasterone B and (F) Protein-pyrrocidine A.

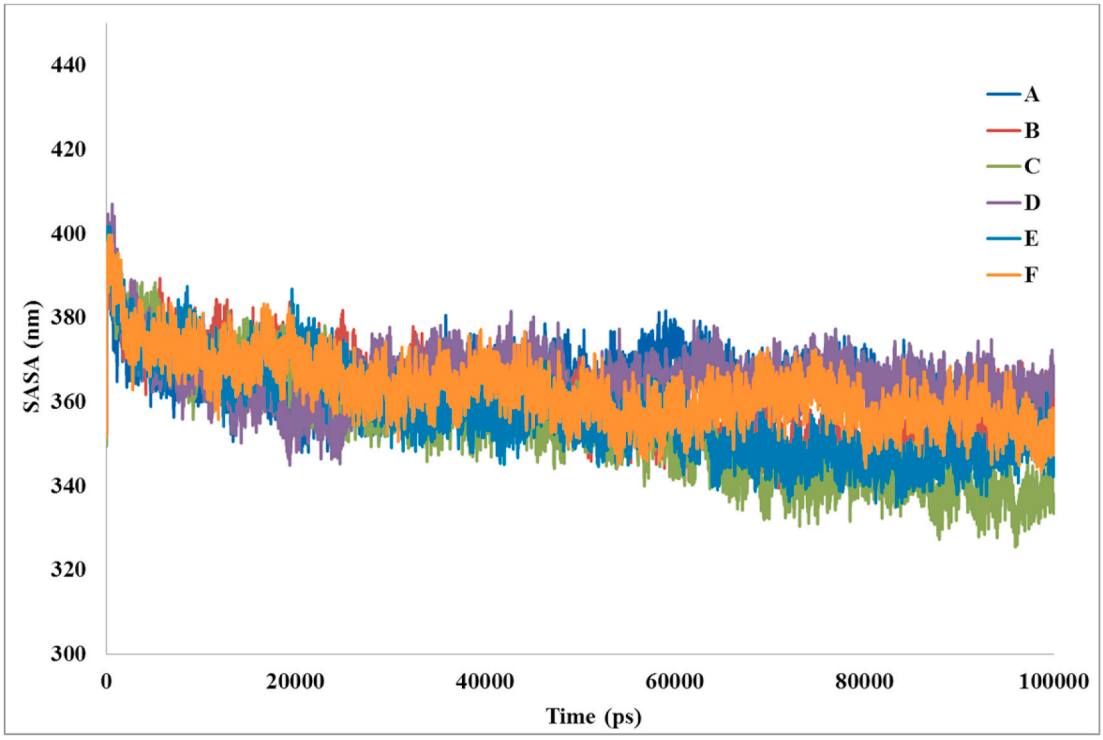

Fig. 6. The SASA analysis of protein in interaction with different ligands (A) free protein, (B) Protein-18-methoxy cytochalasin J, complex C) Protein- (22E,24R)-stigmasta-5,7,22-trien-3-β-ol complex, (D) Protein-beauvericin complex, (E) Protein-dankasterone b complex and (F) Protein-pyrrocidine A complex.

Such striking fluctuations in protein can lead to instability in protein structure and disturb enzymatic activity.

Furthermore, solvent-accessible surface area (SASA) was analyzed for diverse protein-ligand complexes along with that of free nsp12. According to Fig. 6, during the simulation time in all systems, the SASA value decreased. This can be because of both compactness in the protein structure and/or the closing of the water inlet valves of the internal cavities which prevent water from diffusing into the internal parts of the protein. The results also are in agreement with those of Rg and both together confirm that protein undergoes structural compression in an aqueous medium.

The main component of protein movements can be extracted using principal component analysis (PCA). These fundamental movements of any macromolecule play an important role in protein structure and function and any change in their patterns can lead to protein malfunction and/or dysfunction. The 2D patterns of RdRp motions in distinct

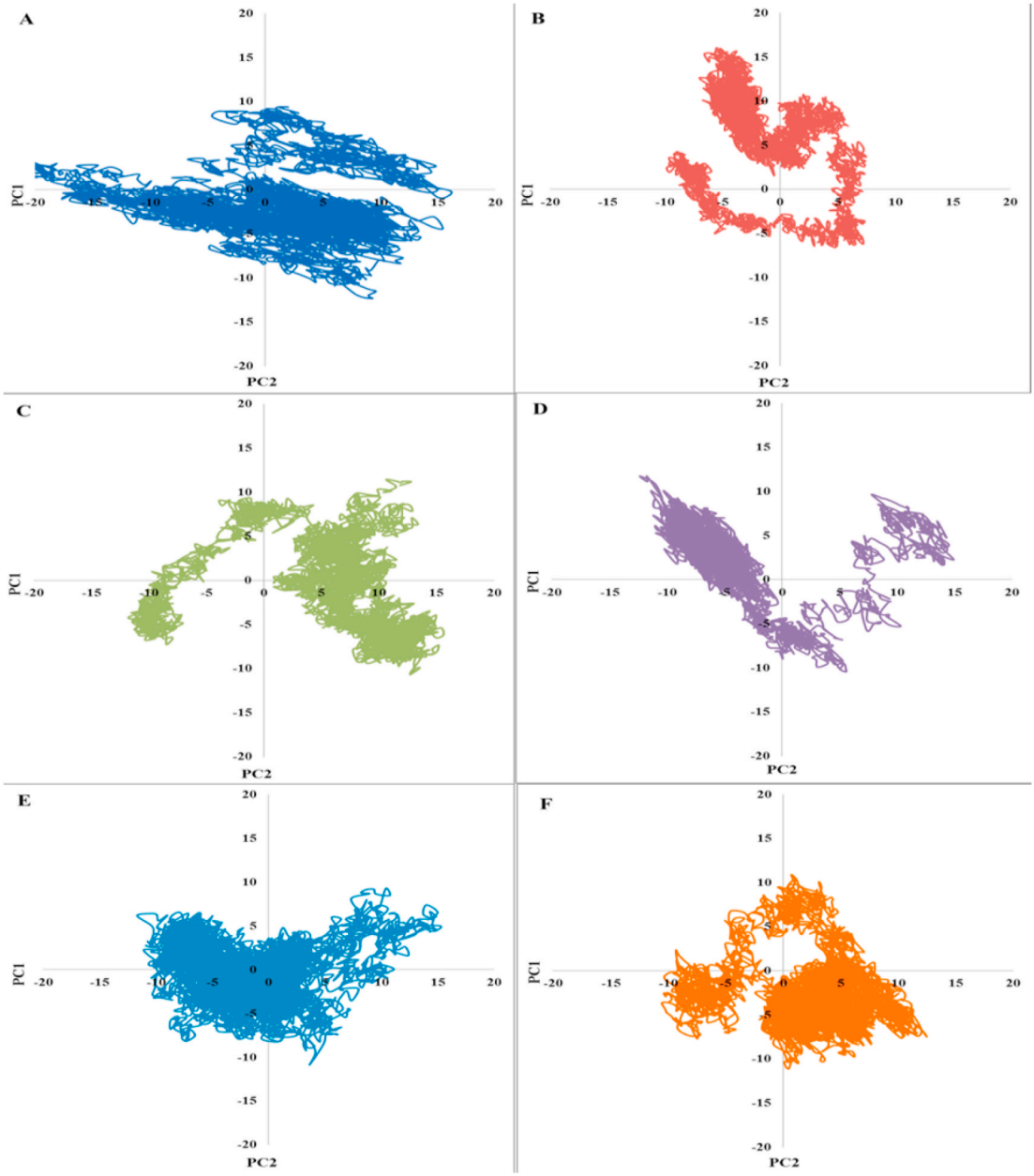

Fig. 7. Comparison of changes in PCA pattern of protein in interaction with different ligands for malfunction (A) free protein, (B) Protein-18-methoxy cytochalasin J, complex C) Protein- (22E,24R)-stigmasta-5,7,22-trien-3-β-ol complex, (D) Protein-beauvericin complex, (E) Protein-dankasterone B complex and (F) Protein-pyrrocidine A complex.

ligand-binding conditions were extracted by PCA and their results are demonstrated in Fig. 7.

As could be seen in Fig. 7A, free protein contains three distinct movement clusters with a relatively large range of motion from −20 to 15 nm. All examined fungal metabolites have altered both the pattern and range of the main protein movement indicating that the compounds can induce instability and malfunction in protein structure and activity. The most severe deformity in pattern and closure in protein mobility is related to 18-MCJ, (22E,24R)-stigmasta-5,7,22-trien-3-β-ol, and pyrrocidine A. This limitation in movement range is in agreement with the findings of Rg indicating that the 3D conformation of viral RdRp undergoes shrinking in the presence of fungal compounds. Such compactness in the protein structure can prevent its accurate interaction with the substrate.

Table 3
The mean interaction energies and hydrogen bondings of drug binding to protein in dynamic state.

	vdW (kj/mol)	Elec (kj/mol)	Total (kj/mol)	Hbond
18-methoxy cytochalasin J	−157.37	−118.51	−275.89	2.06
(22E,24R)-stigmasta-5,7,22-trien-3-β-ol	−113.20	−17.70	−130.91	0.25
Beauvericin	−309.88	−37.75	−347.63	0.49
Dankasterone B	−146.89	−38.18	−185.07	1.36
Pyrrocidine A	−162.47	−50.50	−212.97	1.11

Define Secondary Structure of Proteins (DSSP) is a program for analyzing the change in the secondary structure of studied protein and investigating their alterations as a result of diverse conditions, such as the binding of a ligand. Comparative results of DSSP analysis on different systems are illustrated in Supplementary Figs. S1–S5. The compound 18-MCJ makes unstable an alpha helix in 485–495 and two

Table 4
Drug likeliness of 5 final ligands (Swissadme).

No.	Compound	Lipinski	Ghose	Veber	Egan	Muegge	Bioavailability score
1	18-methoxy cytochalasin J	Yes	No	Yes	No	No	0.55
2	(22E,24R)-stigmasta-5,7,22-trien-3-β-ol	No	Yes	No	No	No	0.55
3	Beauvericin	No	No	Yes	Yes	No	0.17
4	Dankasterone B	Yes	No	Yes	No	No	0.55
5	Pyrrocidine A	Yes	No	Yes	Yes	No	0.55

Table 5
Pharmacological properties and toxisity prediction results for 5 top ligands.

No.	Compound	GI absorption	BBB permeation	P-glycoprotein substrate	CYP1A2 inhibitor	CYP2C19 inhibitor	CYP2C9 inhibitor	CYP2D6 inhibitor	CYP3A4 inhibitor	LD 50 mg/kg
1	18-methoxy cytochalasin J	High	Yes	Yes	No	No	No	No	No	200
2	(22E,24R)-stigmasta-5,7,22-trien-3-β-ol	Low	No	Yes	No	No	No	No	No	500
3	Beauvericin	High	Yes	Yes	No	No	No	No	No	600
4	Dankasterone B	Low	No	Yes	No	No	Yes	No	No	2000
5	Pyrrocidine A	High	Yes	Yes	No	No	Yes	No	No	1980

beta-sheets in locations 420–430 and 440–450 (Fig. S1). In the case of binding (22E,24R)-stigmasta-5,7,22-trien-3-β-ol to protein, the helix in 485–495 was destroyed and another helix in 330–340 was unstable (Fig. S2). Beauvericin destroyed a beta-sheet at the residue position of 635–645 (Fig. S3). An alpha helix in 265–275 was destructed following the binding of dankasterone B to the protein (Fig. S4). Adding pyrrocidine A to RdRp destroyed the c terminal alpha-helix at position 780–790 (Fig. S5).

Binding energies extracted from the dynamic state of interaction obtained by the Molecular Mechanics/Poisson-Boltzmann Surface Area (MM/PBSA) method were calculated and results are shown in Table 3.

Among the simulated compounds, the highest interaction energy was related to Beauvericin, 18-MCJ, and Pyrrocidine A, respectively. Except for the 18-MCJ that contains the highest number of H bonding, the major component of the binding energy is derived from the Van der Waals forces in all RdRp-metabolite interactions.

The five finally selected fungal metabolites were pharmacokinetically assessed using the SwissADME server. As shown in Tables 4 and 5, 18-MCJ and Pyrrocidine A had better pharmacokinetic properties, such as druglikeness and pharmacological characteristics. Our results revealed no drug interactions with other medications for 18-MCJ. However, because of the inhibitory effect of Pyrrocidine A on CYP2C9, it is predicted to have interaction with the metabolism of some common non-steroidal anti-inflammatory drugs and Sulfonylurea (Cytochrome P450 2C9-CYP2C9). Both compounds have high gastrointestinal absorption and can pass the blood-brain barrier. Passing the cell membrane is also important for the compounds to enter the infected cells and reach successfully the viral RdRp. All these features together indicate that both 18-MCJ and Pyrrocidine A can be effectively absorbed, distribute, and diffuse through the body.

Finally, the toxicity of five final fungal metabolites was predicted using ProTox-II online tool and the results are reported in Table 5. As it can be observed, except for 18-MCJ, other compounds had moderate or light toxicity with Dankasterone B and Pyrrocidine A showing higher LD50 than others. Based on the results of the present study, it can be concluded that Dankasterone B and Pyrrocidine A are more suitable candidates than others to be evaluated in experimental studies against COVID-19.

4. Conclusions

In the current study, the inhibitory potential of ninety-nine secondary metabolites extracted from endophytic fungi was computationally evaluated against new coronavirus RNA-dependent RNA polymerase. Following a blind docking on the whole RdRp protein, another targeted docking was carried out on the active site of the enzyme. The five potent compounds with the highest binding energy and maximum number in clusters included 18-methoxy cytochalasin J (MCJ), (22E,24R)-stigmasta-5,7,22-trien-3-β-ol, beauvericin, dankasterone B, and pyrrocidine A. next, the mentioned compounds were selected for molecular dynamics simulation to investigate the dynamic of interaction. The highest value of RMSD was observed in the system containing 18-MCJ, as well as more fluctuations in the presence of dankasterone B. All metabolites changed the value of residue fluctuations at various parts of the protein. Concerning the protein in complex with beauvericin, other systems underwent severe conformation compression extracted from Rg results. The value and pattern of the main components of protein movements changed significantly, especially in the presence of 18-MCJ, (22E,24R)-stigmasta-5,7,22-trien-3-β-ol, and beauvericin. The results of binding energy obtained from the MMPBSA method revealed that the total binding energy of the complexes of RdRp with 18-MCJ, beauvericin, and pyrrocidine A were much more stable than the other two metabolites. Moreover, the ADME features of final compounds were obtained for assessing the pharmacokinetic properties of metabolites. Our findings indicated that 18-MCJ and pyrrocidine A were the most suitable compounds regarding drug pharmacokinetics. According to the results of the present investigation, it is confirmed that dankasterone B and pyrrocidine A fungal secondary metabolites are more potent inhibitors of viral RdRp than other compounds and can be used in further experimental studies to obtain effective anti-coronavirus compounds.

Declaration of competing interest

All authors confirm that there is no any conflict of declaration interests.

Acknowledgments

The authors have acknowledged Kermanshah University of Medical Sciences, Kermanshah, Iran for financial supports; [Grant number 4000118].

Appendix A. Supplementary data

Supplementary data to this article can be found online at https://doi.org/10.1016/j.compbiomed.2021.104613.

References

[1] A. Spinelli, G. Pellino, COVID-19 pandemic: perspectives on an unfolding crisis, Br. J. Surg. (2020).

[2] A. Gupta, M.V. Madhavan, K. Sehgal, N. Nair, S. Mahajan, T.S. Sehrawat, B. Bikdeli, N. Ahluwalia, J.C. Ausiello, E.Y. Wan, Extrapulmonary manifestations of COVID-19, Nat. Med. 26 (2020) 1017–1032.

[3] N. Raffaele, L.L. Carucci, T. Flavia, COVID-19 and ocular implications: an update, Journal of Ophthalmic Inflammation and Infection 10 (2020).

[4] A.A. Elfiky, SARS-CoV-2 RNA dependent RNA polymerase (RdRp) targeting: an in silico perspective, J. Biomol. Struct. Dyn. (2020) 1–9.

[5] S. Ezzikouri, J. Nourlil, S. Benjelloun, M. Kohara, K. Tsukiyama-Kohara, Coronavirus Disease 2019—Historical Context, Virology, Pathogenesis, Immunotherapy, and Vaccine Development, Human vaccines & immunotherapeutics, 2020, pp. 1–9.

[6] A.J. Te Velthuis, J.J. Arnold, C.E. Cameron, S.H. van den Worm, E.J. Snijder, The RNA polymerase activity of SARS-coronavirus nsp12 is primer dependent, Nucleic Acids Res. 38 (2010) 203–214.

[7] H. Jia, P. Gong, A structure-function diversity survey of the RNA-dependent RNA polymerases from the positive-strand RNA viruses, Front. Microbiol. 10 (2019) 1945.

[8] Y. Jiang, W. Yin, H.E. Xu, RNA-dependent RNA Polymerase: Structure, Mechanism, and Drug Discovery for COVID-19, Biochemical and Biophysical Research Communications, 2020.

[9] Y. Gao, L. Yan, Y. Huang, F. Liu, Y. Zhao, L. Cao, T. Wang, Q. Sun, Z. Ming, L. Zhang, Structure of the RNA-dependent RNA polymerase from COVID-19 virus, Science 368 (2020) 779–782.

[10] S. Kumar, N. Kaushik, Metabolites of endophytic fungi as novel source of biofungicide: a review, Phytochemistry Rev. 11 (2012) 507–522.

[11] N.P. Keller, G. Turner, J.W. Bennett, Fungal secondary metabolism—from biochemistry to genomics, Nat. Rev. Microbiol. 3 (2005) 937–947.

[12] N.P. Keller, Fungal secondary metabolism: regulation, function and drug discovery, Nat. Rev. Microbiol. 17 (2019) 167–180.

[13] H.W. Zhang, Y.C. Song, R.X. Tan, Biology and chemistry of endophytes, Nat. Prod. Rep. 23 (2006) 753–771.

[14] E. Tazikeh-Lemeski, S. Moradi, R. Raoufi, M. Shahlaei, M.A.M. Janlou, S. Zolghadri, Targeting SARS-COV-2 non-structural protein 16: a virtual drug repurposing study, J. Biomol. Struct. Dyn. (2020) 1–14.

[15] S. Mandal, S.K. Mandal, Rational drug design, Eur. J. Pharmacol. 625 (2009) 90–100.

[16] M. Ansari, S. Moradi, M. Shahlaei, A molecular dynamics simulation study on the mechanism of loading of gemcitabine and camptothecin in poly lactic-co-glycolic acid as a nano drug delivery system, J. Mol. Liq. 269 (2018) 110–118.

[17] S. Moradi, E. Hosseini, M. Abdoli, S. Khani, M. Shahlaei, Comparative molecular dynamic simulation study on the use of chitosan for temperature stabilization of interferon αII, Carbohydr. Polym. 203 (2019) 52–59.

[18] S. Moradi, S. Khani, M. Ansari, M. Shahlaei, Atomistic details on the mechanism of organophosphates resistance in insects: insights from homology modeling, docking and molecular dynamic simulation, J. Mol. Liq. 276 (2019) 59–66.

[19] Y. Zhou, F. Wang, J. Tang, R. Nussinov, F. Cheng, Artificial intelligence in COVID-19 drug repurposing, The Lancet Digital Health (2020).

[20] B. Shah, P. Modi, S.R. Sagar, in: In Silico Studies on Therapeutic Agents for COVID-19: Drug Repurposing Approach, Life Sciences, 2020, p. 117652.

[21] X. Wang, Y. Guan, COVID-19 Drug Repurposing: A Review of Computational Screening Methods, Clinical Trials, and Protein Interaction Assays, Medicinal Research Reviews, 2020.

[22] J. Wang, Fast identification of possible drug treatment of coronavirus disease-19 (COVID-19) through computational drug repurposing study, J. Chem. Inf. Model. (2020).

[23] Q. Wang, M. Li, X. Wang, N. Parulian, G. Han, J. Ma, J. Tu, Y. Lin, H. Zhang, W. Liu, Covid-19 Literature Knowledge Graph Construction and Drug Repurposing Report Generation, 2020 arXiv preprint arXiv:2007.00576.

[24] S.J. Weiner, P.A. Kollman, D.A. Case, U.C. Singh, C. Ghio, G. Alagona, S. Profeta, P. Weiner, A new force field for molecular mechanical simulation of nucleic acids and proteins, J. Am. Chem. Soc. 106 (1984) 765–784.

[25] G.M. Morris, D.S. Goodsell, R.S. Halliday, R. Huey, W.E. Hart, R.K. Belew, A. J. Olson, Automated docking using a Lamarckian genetic algorithm and an empirical binding free energy function, J. Comput. Chem. 19 (1998) 1639–1662.

[26] E. Lindahl, B. Hess, D. Van Der Spoel, Gromacs 3.0: a package for molecular simulation and trajectory analysis, Molecular modeling annual 7 (2001) 306–317.

[27] A.W. Schüttelkopf, D.M. Van Aalten, PRODRG: a tool for high-throughput crystallography of protein–ligand complexes, Acta Crystallogr. Sect. D Biol. Crystallogr. 60 (2004) 1355–1363.

[28] S.P. Hirshman, J. Whitson, Steepest-descent moment method for three-dimensional magnetohydrodynamic equilibria, Phys. Fluids 26 (1983) 3553–3568.

[29] B. Hess, H. Bekker, H.J. Berendsen, J.G. Fraaije, LINCS: a linear constraint solver for molecular simulations, J. Comput. Chem. 18 (1997) 1463–1472.

[30] W.F. Van Gunsteren, H.J. Berendsen, A leap-frog algorithm for stochastic dynamics, Mol. Simulat. 1 (1988) 173–185.

[31] S. Genheden, U. Ryde, The MM/PBSA and MM/GBSA methods to estimate ligand-binding affinities, Expet Opin. Drug Discov. 10 (2015) 449–461.

[32] R.A. Laskowski, M.B. Swindells, LigPlot+: Multiple Ligand–Protein Interaction Diagrams for Drug Discovery, ACS Publications, 2011.

[33] P. Banerjee, A.O. Eckert, A.K. Schrey, R. Preissner, ProTox-II: a webserver for the prediction of toxicity of chemicals, Nucleic Acids Res. 46 (2018) W257–W263.

[34] X. Xu, Y. Liu, S. Weiss, E. Arnold, S.G. Sarafianos, J. Ding, Molecular model of SARS coronavirus polymerase: implications for biochemical functions and drug design, Nucleic Acids Res. 31 (2003) 7117–7130.